Toward a Preferred 4×4 Space-Time Block Code: A Performance-Versus-Complexity Sweet Spot with Linear-Filter Decoding

Sandipan Kundu, Dimitris A. Pados, *Member IEEE,* Weifeng Su, *Member IEEE,* and Rohan Grover, *Member IEEE*

***Abstract*—We develop a new 4×4 Hadamard-precoded quasi-orthogonal space-time block code (QO-STBC) that enables highly effective near-maximum-likelihood (near-ML) reliability-based prioritized symbol detection using linear filters. Approximate block-error-rate minimization is being used to optimize the code rotation angle. Detailed computational complexity evaluation of the decoder in terms of real multiplications and additions shows significant complexity reduction for symbol alphabet sizes of interest. Numerical and simulation studies demonstrate negligible bit-error-rate degradation compared to the state-of-the-art in bit-error-rate by ML decoded 4×4 codewords.**

***Index Terms*—Hadamard precoding, matched-filter (MF), maximum-likelihood (ML) detection, minimum-mean-square-error (MMSE) filter, multi-input multi-output (MIMO) communications, quasi-orthogonal space-time block codes (QO-STBC).**

I. Introduction

ORTHOGONAL space-time block codes (O-STBC) [1] offer full transmit diversity and allow disjoint single-complex-symbol maximum-likelihood (ML) decoding. The first-in-line, celebrated 2-transmit-antenna Alamouti O-STBC [2] has also rate one and ushered wireless communications in the era of space-time coded transmissions. Full-diversity, rate-one O-STBCs for complex symbols drawn from arbitrary constellations do not exist, however, for systems with more than two transmit antennas [1], [3]. For systems with four transmit antennas, a case of great practical importance, the rate limitation of O-STBCs was overcome by quasi-orthogonal space-time block codes (QO-STBCs) [4]-[8] at the expense of diversity loss and increased decoding complexity. Rotation of few symbols in the QO-STBC can, however, reinstate full-diversity. In particular, full-diversity rate-one QO-STBCs for 4-transmit-antennas were described in [9]-[14]. On the other hand, ML decoding of the full-diversity QO-STBCs in [9], [10] requires joint detection of two complex symbols (four real symbols), which is computationally expensive for high-order signal constellations. In [11], interleaving real and imaginary parts of rotated symbols enables single-symbol decoding of full-rate full-diversity QO-STBCs for the 4-transmit-antenna case. Linear-transformation-based full-diversity QO-STBCs with joint two-real-symbol ML decoding were presented in [12], [13]. Grouping of dispersion matrices leading to joint two-real-symbol ML decodable full-diversity codewords was described in [14]. Noise prewhitening followed by subgroup ML decoding was suggested in [15].

Arguably, the practical significance of a high-performing low-computational-complexity 4×4 space-time code warrants further research. Recently, low complexity block-orthogonal [16], [17] and several other general proposals appeared in the literature on linear (or partial-interference-cancelation (PIC)) receivers of space-time codes [18]-[20], but have not provided yet an appealing definitive solution for the 4 transmit antenna case.

In this paper, we develop a new (open-loop) Hadamard precoded 4×4 QO-STBC codeword that, unlike codewords from [11]-[15], facilitates high-performance reliability-based linear-complexity decoding using minimum-mean-square-error (MMSE) and matched filters (MF). Precoded codewords and linear receivers were also pursued earlier on by Sezgin and Oechtering [21] with resulting error rates that may be deemed, however, unsatisfactory. For the developed codeword herein[1] and the MMSE-MF decoder, a semi-closed-form approximate block-error-rate expression is derived, which is then minimized to find the optimal codeword rotation angle. Simulation and numerical studies are, then, provided to compare the error rate of the proposed code under ML and MMSE-MF decoding and existing works in the literature. The tradeoff performance-versus-complexity point becomes, arguably, the most appealing to date in view of the minimal computational cost per decoding measured in number of real multiplications and additions executed by the described scheme.

The rest of the paper is organized as follows. In Section II, the system model and necessary notation for the proposed codeword is introduced. In Section III, we derive the proposed associated linear-filter (MMSE-MF) detector. Performance optimization for the MMSE-MF detector is carried out in Section IV. Complexity and error rate performance comparisons are presented in Section V. A few concluding remarks are drawn in Section VI.

Manuscript received May 17, 2012; revised October 14 and December 13, 2012. The associate editor coordinating the review of this paper and approving it for publication was M. Matthaiou.

S. Kundu, D. A. Pados, and W. Su are with the COMSENS Research Center, Dept. of Electrical Engineering, State University of New York at Buffalo, Buffalo, NY, 14260, USA (e-mail: {skundu, pados, weifeng}@buffalo.edu).

R. Grover is with Mirics, Needham, MA, 02494, USA (e-mail: rohan.grover@mirics.com).

This paper was presented in part at the IEEE Wireless Communications and Networking Conference (WCNC), Paris, France, April 2012.

Digital Object Identifier 10.1109/TCOMM.2013.021913.120338

[1]The proposed precoded codeword enjoys full-diversity under joint two-real symbol ML decoding as in the works of [11]-[14].

II. System Model

Throughout this paper, we use the following notation: $\mathbb{E}\{\cdot\}$ denotes statistical expectation; $(\mathbf{B})^{-1}$, $\|\mathbf{B}\|_2^2$, $\mathbf{B}^T$, $\mathbf{B}^H$, $[\mathbf{B}]_{i,j}$ denote the inverse, L_2 norm, transpose, Hermitian, and (i,j)th element of matrix $\mathbf{B}$; $\mathbf{I}_L$, $\mathbf{0}_L$ is the identity and all zero matrix of size L; $(\cdot)^*$ is the complex conjugation operator and $Re\{\cdot\}$ extracts the real part of a complex number.

We consider a system with $M_t = 4$ transmit antennas and $T = 4$ time slots over which the space-time code is to be transmitted (4×4 space-time block coding). For ease in presentation, we consider the system case of one receive antenna, $M_r = 1$. The treatment is, of course, directly extendable to any number of receive antennas. We assume perfect channel state information (CSI) at the receiver and no CSI at the transmitter. The independent symbols to be transmitted are formed by mapping the incoming bits onto a known unit energy signal constellation $\mathcal{A}$ (for example, quadrature amplitude modulation (QAM)) to form symbols $z_1, \cdots, z_4$, which are then represented by a column vector $\mathbf{z}$. The symbol vector $\mathbf{z}$ is precoded by the Hadamard matrix $\mathbf{V}$ of size 4 followed by the diagonal rotation matrix operator $\mathbf{P}_\theta \triangleq \begin{bmatrix} \mathbf{I}_2 & \mathbf{0}_2 \\ \mathbf{0}_2 & e^{j\theta}\mathbf{I}_2 \end{bmatrix}$, $\theta \in [0, \pi/2]$, to form the final precoded symbol vector $\mathbf{x}$ with elements $x_1, \cdots, x_4$,

$$\mathbf{x} = \mathbf{P}_\theta \frac{\mathbf{V}}{2}\mathbf{z} \tag{1}$$

where the factor $\frac{1}{2}$ is the energy normalization constant to make each symbol of unit energy and θ in $\mathbf{P}_\theta$ is the rotation angle to be optimized. The final space-time block code matrix of size four-by-four to be transmitted has the structure [5], [9]

$$\mathbf{X} = \begin{bmatrix} x_1 & x_2 & x_3 & x_4 \\ -x_2^* & x_1^* & -x_4^* & x_3^* \\ x_3 & x_4 & x_1 & x_2 \\ -x_4^* & x_3^* & -x_2^* & x_1^* \end{bmatrix}. \tag{2}$$

The received signal $\mathbf{y}$ of size $(T = 4) \times (M_r = 1)$ is given by

$$\mathbf{y} = \sqrt{\frac{\rho}{M_t}}\mathbf{X}\mathbf{h} + \mathbf{n} \tag{3}$$

where ρ is the signal-to-noise ratio (SNR) per receive antenna, $\mathbf{h}$ is the channel vector with elements $h_1, \cdots, h_4$, and $\mathbf{n}$ is the additive noise vector. The channel is assumed to be quasi-static with Rayleigh fading coefficients. The elements of $\mathbf{h}$ and $\mathbf{n}$, h_i, n_l, $1 \le i \le M_t$, $1 \le l \le T$, respectively, are being modeled as independent and identically distributed complex Gaussian random variables with zero mean and unit variance. The channel-equivalent representation of (3) is given by [10], [21] (see also [22])

$$\mathbf{y}_e = \sqrt{\frac{\rho}{4M_t}}\mathbf{H}\mathbf{V}\mathbf{z} + \mathbf{n}_e \tag{4}$$

where $\mathbf{y}_e, \mathbf{n}_e$ are obtained by conjugating the second and fourth element of $\mathbf{y}$ and $\mathbf{n}$ respectively, and

$$\mathbf{H} \triangleq \begin{bmatrix} h_1 & h_2 & h_3 & h_4 \\ h_2^* & -h_1^* & h_4^* & -h_3^* \\ h_3 & h_4 & h_1 & h_2 \\ h_4^* & -h_3^* & h_2^* & -h_1^* \end{bmatrix} \mathbf{P}_\theta \tag{5}$$

is the equivalent channel matrix. The Hadamard precoding operation by $\mathbf{V}$ enables us to derive and propose two low-complexity detectors as discussed in the following section, a joint two-real-symbol ML decoder and a two-stage MMSE-MF decoder. We will suggest that the latter offers the best performance-versus-complexity tradeoff known to date.

III. Decoders

In this section, we derive and discuss an ML and a linear-filter decoder for the received signal vector $\mathbf{y}_e$ in (4).

A. Joint Two-real-symbol ML Decoding

With knowledge of CSI and the fixed precoder $\mathbf{V}$ at the receiver, the ML decoder of $\mathbf{z}$ requires 4 independent joint two-real-symbol decoding as opposed to joint decoding of 4 complex symbols. The ML decoder for the signal in (4) is given by

$$\begin{aligned} \hat{\mathbf{z}}_{ML} &= \arg\min_{\mathbf{z}\in\mathcal{A}} \|\mathbf{y}_e - \sqrt{\frac{\rho}{4M_t}}\mathbf{H}\mathbf{V}\mathbf{z}\|_2^2 \\ &= \arg\min_{\mathbf{z}\in\mathcal{A}} \Big[-2\, Re\Big\{\mathbf{y}_e^H \mathbf{H}\mathbf{V}\mathbf{z}\Big\} \\ &\qquad + \sqrt{\frac{\rho}{4M_t}}\mathbf{z}^H\mathbf{V}^H\mathbf{H}^H\mathbf{H}\mathbf{V}\mathbf{z} \Big]. \end{aligned} \tag{6}$$

Analyzing cross-interference terms will allow us to identify symbol couplings for ML decoding. Simplifying the second term in (6) and ignoring the multiplicative constant we obtain

$$\begin{aligned} \mathbf{z}^H\mathbf{V}^H\mathbf{H}^H\mathbf{H}\mathbf{V}\mathbf{z} &= \mathbf{z}^H \begin{bmatrix} (a+b\cos\theta)\mathbf{I}_2 & -jb\sin\theta\ \mathbf{I}_2 \\ jb\sin\theta\ \mathbf{I}_2 & (a-b\cos\theta)\mathbf{I}_2 \end{bmatrix} \mathbf{z} \\ &= \mathbf{z}_{13}^H \begin{bmatrix} (a+b\cos\theta) & -jb\sin\theta \\ jb\sin\theta & (a-b\cos\theta) \end{bmatrix} \mathbf{z}_{13} \\ &\quad + \mathbf{z}_{24}^H \begin{bmatrix} (a+b\cos\theta) & -jb\sin\theta \\ jb\sin\theta & (a-b\cos\theta) \end{bmatrix} \mathbf{z}_{24} \end{aligned} \tag{7}$$

where $\mathbf{z}_{13} \triangleq [z_1\ z_3]^T$, $\mathbf{z}_{24} \triangleq [z_2\ z_4]^T$, and $a \triangleq \sum_{i=1}^{4} |h_i|^2$, $b \triangleq 2Re\{h_1h_3^* + h_2h_4^*\}$ are channel dependent constants known to the receiver. As the two terms in (7) are identical, we expand the first term only to study the inter-symbol-interference

$$\begin{aligned} \mathbf{z}_{13}^H \begin{bmatrix} (a+b\cos\theta) & -jb\sin\theta \\ jb\sin\theta & (a-b\cos\theta) \end{bmatrix} \mathbf{z}_{13} &= |z_1|^2(a+b\cos\theta) + \\ |z_3|^2(a-b\cos\theta) &+ 2b\sin\theta(z_{1R}z_{3I} - z_{1I}z_{3R}) \end{aligned} \tag{8}$$

where the subscripts R and I denote real and imaginary part, respectively. As shown above, inter-symbol-interference exists between symbol pairs (z_1, z_3) and (z_2, z_4), while the two groups of symbols are orthogonal to each other. Furthermore, in each pair the real and imaginary part of the symbols do not interfere with each other. For the pair (z_1, z_3), interference exists between real symbols (z_{1R}, z_{3I}) and (z_{1I}, z_{3R}); for the pair (z_2, z_4) interference exists between real symbols (z_{2R}, z_{4I}) and (z_{2I}, z_{4R}). Thus, ML decoding of (4) requires joint decoding of the real and imaginary part of the two different symbols (i.e., two-real-symbol decoding) resulting in the same decoding complexity as in [11]-[14]. The ML decoding equations are given at the top of the next page, where $\alpha = \mathbf{y}_e^H\mathbf{H}\mathbf{V}$, $\beta_{k,R}$ and $\beta_{k,I}$, $k = 1, 2$, are the real

$$(\hat{z}_{k,R}, \hat{z}_{k+2,I}) = \underset{\substack{z_{k,R}\in\mathcal{A}_R \\ z_{k+2,I}\in\mathcal{A}_I}}{\arg\min} \Big[(a+b\cos\theta)z_{k,R}^2 + (a-b\cos\theta)z_{k+2,I}^2 - (2b\sin\theta)z_{k,R}\, z_{k+2,I} + \alpha_{k,R}\, z_{k,R} - \alpha_{k+2,I} z_{k+2,I}\Big]$$

$$(\hat{z}_{k,I}, \hat{z}_{k+2,R}) = \underset{\substack{z_{k,I}\in\mathcal{A}_I \\ z_{k+2,R}\in\mathcal{A}_R}}{\arg\min} \Big[(a+b\cos\theta)z_{k,I}^2 + (a-b\cos\theta)z_{k+2,R}^2 - (2b\sin\theta)z_{k,I}\, z_{k+2,R} - \alpha_{k,I}\, z_{k,I} + \alpha_{k+2,R} z_{k+2,R}\Big]$$

and imaginary part of a complex number, and $\mathcal{A}_R$ and $\mathcal{A}_I$ are the set of real and imaginary parts of the signal constellation $\mathcal{A}$.

The codeword in (1), (2) achieves full-diversity under ML decoding as can be easily shown by following the analysis of [9].

B. MMSE-MF Decoding

Next, we derive and describe in detail a reliability based two-stage linear-filter decoding approach. In stage one, we will adaptively choose two symbols to be MMSE decoded and removed. Then, in stage two, the two remaining symbols will be MF decoded.

The incorporated Hadamard precoding in (1), (2) bestows different signal-to-interference-plus-noise ratio (SINR) at the output of the MMSE filter for different symbols. The symbols having higher SINR (reliability) are to be decoded first and removed from the linearized received signal $\mathbf{y}_e$. The remaining symbols are to be decoded at the second stage with simple channel MF filters. The first step of the decoder is to determine which of the symbols will have higher SINR and will be decoded at the first stage with the MMSE filter. To answer this question that lies in the core of this work, we calculate the post MMSE filtering SINR and show that a simple channel parameter can be used to determine the symbols having higher SINR.

For the received signal model in (4) the MMSE filter (in matrix form) is given by

$$\mathbf{W} = \sqrt{\frac{\rho}{4M_t}}(\mathbf{HV})\Big(\mathbf{I}_4 + \frac{\rho}{4M_t}\mathbf{V}^H\mathbf{H}^H\mathbf{HV}\Big)^{-1}.$$

The MMSE receiver output is

$$\hat{\mathbf{z}} = \mathbf{W}^H\mathbf{y_e}.$$

The post-filtering SINRs are

$$\text{SINR}_\ell = \frac{1}{\Big[\Big(\mathbf{I}_4 + \frac{\rho}{4M_t}\mathbf{V}^H\mathbf{H}^H\mathbf{HV}\Big)^{-1}\Big]_{\ell,\ell}} - 1, \quad \ell = 1, \cdots, 4,$$

where $[\mathbf{B}]_{i,j}$ represents the element in the i^{th} row and j^{th} column of matrix $\mathbf{B}$. Simplifying SINR_ℓ further, we obtain

$$\text{SINR}_\ell = \frac{\Big(\frac{\rho}{M_t}a + 1\Big)^2 - \Big(\frac{\rho}{M_t}b\Big)^2}{\frac{\rho}{Mt}\Big(a - b\cos\theta\Big) + 1} - 1, \ \ell = 1, 2, \text{ and} \qquad (9)$$

$$\text{SINR}_\ell = \frac{\Big(\frac{\rho}{M_t}a + 1\Big)^2 - \Big(\frac{\rho}{M_t}b\Big)^2}{\frac{\rho}{Mt}\Big(a + b\cos\theta\Big) + 1} - 1, \ \ell = 3, 4. \qquad (10)$$

Hence, by the Hadamard precoding, one symbol in each pair (z_1, z_3) and (z_2, z_4) has higher SINR than the other. From (9), (10), we conclude that out of the four symbols in a codeword, two of the symbols have high SINR and the other two have lower SINR, *depending on the channel parameter* b. If $b \geq 0$, symbols z_1, z_2 have higher SINR than z_3, z_4 and are decoded first. If $b < 0$, symbols z_3, z_4 have higher SINR than z_1, z_2 and are decoded first. The proposed MMSE-MF decoder is summarized below where $\mathbf{V}_{[i,j]}$ denotes the submatrix of $\mathbf{V}$ consisting of the i and j columns and $\mathbb{U}(\cdot)$ is the symbol decision operator after linear filtering.

MMSE-MF Decoder

1. Compute sign of $b \triangleq 2Re(h_1h_3^* + h_2h_4^*)$.
2. If $b \geq 0$
   - (i) $(\hat{z}_1, \hat{z}_2) = \mathbb{U}(\mathbf{W}_L^H\mathbf{y}_e)$;
   - (ii) $\mathbf{y}_e^{'} = \mathbf{y}_e - \sqrt{\frac{\rho}{4M_t}}(\mathbf{HV})\,[\hat{z}_1\ \hat{z}_2\ 0\ 0]^T$;
   - (iii) $(\hat{z}_3, \hat{z}_4) = \mathbb{U}\Big((\mathbf{V})_{[3,4]}^H\mathbf{H}^H\mathbf{y}_e^{'}\Big)$.

   else
   - (i) $(\hat{z}_3, \hat{z}_4) = \mathbb{U}(\mathbf{W}_L^H\mathbf{y}_e)$;
   - (ii) $\mathbf{y}_e^{'} = \mathbf{y}_e - \sqrt{\frac{\rho}{4M_t}}(\mathbf{HV})\,[0\ 0\ \hat{z}_3\ \hat{z}_4]^T$;
   - (iii) $(\hat{z}_1, \hat{z}_2) = \mathbb{U}\Big((\mathbf{V})_{[1,2]}^H\mathbf{H}^H\mathbf{y}_e^{'}\Big)$.

   end

We conclude this section on decoding the described codeword with the technical statement that the proposed two-stage MMSE-MF approach is equivalent to an MMSE-MMSE or MMSE-ML configuration, at the lowest computational cost. For brevity in presentation, the equivalence is shown in Appendix A.

IV. Codeword Performance Optimization for MMSE-MF Decoding

In this section, we provide approximate block-error-rate analysis of the MMSE-MF decoder of the proposed codeword in (1), (2) with the aim of finding the optimal (minimum block-error-rate) rotation angle in $\mathbf{P}_\theta$.

We calculate the probability of error for each of the symbol pairs (z_1, z_3) and (z_2, z_4) and then the error rate for the whole codeword. The error rate is calculated stage-wise rather than symbol-wise. As both the pairs have the same probability of error due to the structure of the STBC, any pair of symbols can be chosen to carry out the error rate analysis. We denote by (s_1, s_2) the symbol pair chosen to be detected at the first stage ($(s_1,\ s_2) = (z_1, z_2)$ if $b \geq 0$ and $(s_1,\ s_2) = (z_3, z_4)$ if $b < 0$). The average probability of error of the pair of symbols (s_1, s_2) is given by

$$\begin{aligned}\mathcal{P}_{(s_1,s_2)} &= (1-\mathcal{P}_{L1})\mathcal{P}_{L2} + (1-\mathcal{P}_{L2})\mathcal{P}_{L1} + \mathcal{P}_{L1}\mathcal{P}_{L2} \\ &= \mathcal{P}_{L1} + \mathcal{P}_{L2} - \mathcal{P}_{L1}\mathcal{P}_{L2} \qquad (11)\end{aligned}$$

where $\mathcal{P}_{L1}, \mathcal{P}_{L2}$ ($\mathcal{P}_{L2}$ being a function of $\mathcal{P}_{L1}$) are the average probability of error of the symbols detected with linear MMSE in the first stage and the MF detector in the second stage, respectively.

Symbol s_1 is detected at the first stage with the MMSE filter receiver. The SINR at the output of the MMSE filter at the first stage is

$$\begin{aligned}\gamma_{L1} &= \frac{\left(\frac{\rho}{M_t}a+1\right)^2-\left(\frac{\rho}{M_t}b\right)^2}{\frac{\rho}{Mt}\Big(a-|b|\cos\theta\Big)+1}-1 \\ &= \frac{(\rho/4)^2(a^2-b^2)+(\rho/4)(a+|b|\cos\theta)}{(\rho/4)(a-|b|\cos\theta)+1} \\ &\approx (\rho/4)\frac{a(1-w^2)}{1-w\cos\theta}+\frac{1+w\cos\theta}{1-w\cos\theta} \\ &\geq (\rho/4)\frac{a(1-w^2)}{1-w\cos\theta}+1 \triangleq \tilde{\gamma}_{L1}+1 \qquad (12)\end{aligned}$$

where $w \triangleq |b|/a < 1$. The approximation comes under the consideration of sufficiently large ρ.

Next, we calculate the channel instantaneous symbol error probability at the output of the MMSE filter, denoted by $\mathcal{P}_{L1}^{CSI}$. The instantaneous symbol error probability can be found for many signal constellations in [23]. We focus on square quadrature amplitude modulation (QAM) constellations for illustration purposes only. Other constellations can be easily covered as well (for example phase-shift-keying). For a square QAM constellation of size $|\mathcal{A}| = 2^f$ where f is even, the channel instantaneous symbol error probability is

$$\mathcal{P}_{L1}^{CSI} = 4\mu Q(\sqrt{\delta(\tilde{\gamma}_{L1}+1)}) - 4\mu^2 Q^2(\sqrt{\delta(\tilde{\gamma}_{L1}+1)})$$

where $\mu = 1-\frac{1}{\sqrt{|\mathcal{A}|}}, \delta = \frac{3}{|\mathcal{A}|-1}$ and $Q(\cdot)$ is the Gaussian Q-function. Using the notation

$$\left[\epsilon_1\int_{\eta^L}^{\eta^U} - \epsilon_2\int_{\tau^L}^{\tau^U}\right]F(\varepsilon)d\varepsilon \triangleq \epsilon_1\int_{\eta^L}^{\eta^U}F(\varepsilon)d\varepsilon - \epsilon_2\int_{\tau^L}^{\tau^U}F(\varepsilon)d\varepsilon \quad (13)$$

and the integral representation of the Q-function [23], we can further simplify to

$$\mathcal{P}_{L1}^{CSI} = \left[\frac{4\mu}{\pi}\int_0^{\frac{\pi}{2}} - \frac{4\mu^2}{\pi}\int_0^{\frac{\pi}{4}}\right]e^{-\alpha_1(\phi)}d\phi \qquad (14)$$

where $\alpha_1(\phi) \triangleq \frac{\delta(\tilde{\gamma}_{L1}+1)}{2sin^2\phi}$. We now try to find the average symbol error probability over all channel realizations

$$\mathcal{P}_{L1} = \int \mathcal{P}_{L1}^{CSI} f(\mathbf{h})d\mathbf{h} \qquad (15)$$

where $f(\mathbf{h})$ is the probability density function of the channel vector. Even numerical calculation of $\mathcal{P}_{L1}$ in (15) is hard as it requires executing five-fold integration. The instantaneous SINR parameter $\tilde{\gamma}_{L1}$ in (12) of the MMSE filter output is a function over two real random variables a, w, which in turn are functions of the channel vector $\mathbf{h}$. We derived (shown in Appendix B) the joint distribution of a, w,

$$f_{\mathbf{a},\mathbf{w}}(a,w) = \frac{1}{4}(1-w^2)a^3e^{-a},\ a\in(0,\infty),\ w\in(0,1). \quad (16)$$

Using (16) and (14) in (15),

$$\begin{aligned}\mathcal{P}_{L1} &= \int_0^1\int_0^\infty \mathcal{P}_{L1}^{CSI} f_{\mathbf{a},\mathbf{w}}(a,w)\,da\,dw \\ &= \left[\frac{4\mu}{\pi}\int_0^{\frac{\pi}{2}}\int_0^1\int_0^\infty - \frac{4\mu^2}{\pi}\int_0^{\frac{\pi}{4}}\int_0^1\int_0^\infty\right]e^{-\frac{\delta(\tilde{\gamma}_{L1}+1)}{2sin^2\phi}} f_{\mathbf{a},\mathbf{w}}(a,w)da\,dw\,d\phi \\ &= \left[\frac{4\mu}{\pi}\int_0^{\frac{\pi}{2}}\int_0^1\int_0^\infty - \frac{4\mu^2}{\pi}\int_0^{\frac{\pi}{4}}\int_0^1\int_0^\infty\right]c(\phi)I_1(a,w,\phi)\,da\,dw\,\,d\phi \\ &= \left[\frac{\mu\Gamma(4)}{\pi}\int_0^{\frac{\pi}{2}}\int_0^1 - \frac{\mu^2\Gamma(4)}{\pi}\int_0^{\frac{\pi}{4}}\int_0^1\right]\frac{c(\phi)(1-w^2)}{\Big[G_1(w,\phi)\Big]^4}dw\,d\phi \quad (17)\end{aligned}$$

where we have used $\int_0^\infty x^p e^{-ux}dx = \Gamma(p+1)u^{-(p+1)}$, $p > -1, u > 0$ [24], $I_1(a,w,\phi) \triangleq e^{-\left[\frac{\delta\rho(1-w^2)}{8sin^2\phi(1-w\cos\theta)}+1\right]a}\left\{\frac{a^3(1-w^2)}{4}\right\}$, $c(\phi) \triangleq e^{-\frac{\delta}{2sin^2\phi}}$, $G_1(w,\phi) \triangleq \frac{\delta\rho(1-w^2)}{8sin^2\phi(1-w\cos\theta)} + 1$, and $\Gamma(\cdot)$ is the gamma function in (17). We may further integrate (17) with respect to the variable w, but the result is highly complicated and laborious and does not provide new insight in the analysis of the system. Therefore, the average symbol error probability calculation is left at two-fold integration (from five-fold integration initially).

Next, we calculate the symbol error probability $\mathcal{P}_{L2}$ for the symbol s_2 detected with the MF filter decoder at the second stage. The error rate of the second stage $\mathcal{P}_{L2}$ depends on the error rate of the first stage $\mathcal{P}_{L1}$ and is as follows:

$$\begin{aligned}\mathcal{P}_{L2} &= P_e\Big(\hat{s}_2\neq s_2\Big|\hat{s}_1=s_1\Big)\Big(1-\mathcal{P}_{L1}\Big) \\ &\quad + P_e\Big(\hat{s}_2\neq s_2\Big|\hat{s}_1\neq s_1\Big)\mathcal{P}_{L1} \qquad (18) \\ &\leq P_e\Big(\hat{s}_2\neq s_2\Big|\hat{s}_1=s_1\Big)\Big(1-\mathcal{P}_{L1}\Big)+\mathcal{P}_{L1} \quad (19)\end{aligned}$$

where $\hat{s}_1$ and $\hat{s}_2$ are the symbols detected at the first and second stage, respectively. $P_e\Big(\hat{s}_2 \neq s_2\Big|\hat{s}_1 = s_1\Big)$ is the average probability that the symbol detected at the second stage $\hat{s}_2$ is in error provided that the detected symbol $\hat{s}_1$ at the first stage is correct; $P_e\Big(\hat{s}_2 \neq s_2\Big|\hat{s}_1 \neq s_1\Big)$ is the average probability that the symbol detected at the second stage $\hat{s}_2$ is in error provided that the detected symbol $\hat{s}_1$ in the first stage is also in error. By inspection, (19) provides an upper-bound on the symbol error probability for the second stage. We proceed now with the distinct calculations of $P_e\Big(\hat{s}_2 \neq s_2\Big|\hat{s}_1 = s_1\Big)$ and $P_e\Big(\hat{s}_2 \neq s_2\Big|\hat{s}_1 \neq s_1\Big)$.

Calculation of $P_e\Big(\hat{s}_2 \neq s_2\Big|\hat{s}_1 = s_1\Big) \triangleq \mathcal{P}_{e|\overline{L1}}$

We need to write the received signal expression under the conditions $\hat{s}_2 = s_2$ and $\hat{s}_2 \neq s_2$. The component of the received signal $\mathbf{y}_e$ due to symbols s_1, s_2 is

$$\mathbf{y}_{e12} = \sqrt{\frac{\rho}{4M_t}}\mathbf{H}\mathbf{V}_{[1,3]}\mathbf{J}\begin{bmatrix}s_1\\ s_2\end{bmatrix} + \mathbf{n}_e \qquad (20)$$

where $\mathbf{V}_{[1,3]}$ are the first and third columns of the Hadamard matrix $\mathbf{V}$ and $\mathbf{J}$ is a 2×2 permutation matrix depending on the sign of the channel parameter b. We denote the columns of $\mathbf{H}\mathbf{V}_{[1,3]}\mathbf{J}$ by $\mathbf{g}_1$ and $\mathbf{g}_2$. Under the assumption $\hat{s}_1 = s_1$,

the resulting signal after the removal of the detected symbol at the first stage ($\hat{s}_1$) from $\mathbf{y}_{e12}$ is

$$\mathbf{y}^C_{e12} = \mathbf{y}_{e12} - \sqrt{\frac{\rho}{4M_t}}\mathbf{g}_1\,\hat{s}_1 = \sqrt{\frac{\rho}{4M_t}}\mathbf{g}_2\,s_2 + \mathbf{n}_e. \quad (21)$$

The matched-filter $\mathbf{g}_2$ (second column of $\mathbf{HV}_{[1,3]}$) is used for detecting the symbol s_2 at the second stage with channel instantaneous SNR

$$\gamma^C_{L2} = \frac{\mathbb{E}|\mathbf{g}_2^H\,(\sqrt{\frac{\rho}{4M_t}}\mathbf{g}_2 s_2)|^2}{\mathbb{E}|\mathbf{g}_2^H\,\mathbf{n}_e|^2} = \frac{\rho}{M_t}(a)(1 - w\cos\theta). \quad (22)$$

Following the notation in (13), we simplify the channel instantaneous symbol error probability to

$$\mathcal{P}^{CSI}_{e|\overline{L1}} = \left[\frac{4}{\pi}\mu\int_0^{\frac{\pi}{2}} - \frac{4}{\pi}\mu^2\int_0^{\frac{\pi}{4}}\right] e^{-\alpha_2(\phi)}d\phi \quad (23)$$

where $\alpha_2(\phi) \triangleq \frac{\delta\gamma^C_{L2}}{2\sin^2\phi}$. We now try to find the average symbol error probability at the second stage under $\hat{s}_1 = s_1$ over all channel realizations

$$\begin{aligned}
\mathcal{P}_{e|\overline{L1}} &= \int_0^1\int_0^\infty \mathcal{P}^{CSI}_{e|\overline{L1}} f_{\mathbf{a},\mathbf{w}}(a,w)\,da\,dw \\
&= \left[\frac{4\mu}{\pi}\int_0^{\frac{\pi}{2}}\int_0^1\int_0^\infty - \frac{4\mu^2}{\pi}\int_0^{\frac{\pi}{4}}\int_0^1\int_0^\infty\right] e^{-\frac{\delta\gamma^C_{L2}}{2\sin^2\phi}} f_{\mathbf{a},\mathbf{w}}(a,w)da\,dw\,d\phi \\
&= \left[\frac{4\mu}{\pi}\int_0^{\frac{\pi}{2}}\int_0^1\int_0^\infty - \frac{4\mu^2}{\pi}\int_0^{\frac{\pi}{4}}\int_0^1\int_0^\infty\right] I_2(a,w,\phi)\,da\,dw\,d\phi \\
&= \left[\frac{\mu\Gamma(4)}{\pi}\int_0^{\frac{\pi}{2}}\int_0^1 - \frac{\mu^2\Gamma(4)}{\pi}\int_0^{\frac{\pi}{4}}\int_0^1\right] \frac{(1-w^2)}{\Big[G_2(w,\phi)\Big]^4} dw\,d\phi \quad (24)
\end{aligned}$$

where $I_2(a,w,\phi) \triangleq e^{-\left[\frac{\delta\rho(1-w\cos\theta)}{8sin^2\phi}+1\right]a}\left\{\frac{a^3(1-w^2)}{4}\right\}$, $G_2(w,\phi) \triangleq \frac{\delta\rho(1-w\cos\theta)}{8sin^2\phi} + 1$. As with (17), integrating further is cumbersome without adding much in analysis. Using (17) and (24) in (19), we can obtain the upper-bound on the symbol error probability at the second stage $\mathcal{P}_{L2}$.

Calculation of $P_e\Big(\hat{s}_2 \neq s_2\Big|\hat{s}_1 \neq s_1\Big) \triangleq \mathcal{P}_{e|L1}$

Under the assumption $\hat{s}_1 \neq s_1$, the resulting signal after the removal of the (incorrectly) detected symbol at the first stage ($\hat{s}_1$) from $\mathbf{y}_{\mathbf{e}12}$ is

$$\begin{aligned}
\mathbf{y}^E_{e12} &= \mathbf{y}_{e12} - \sqrt{\frac{\rho}{4M_t}}\mathbf{g}_1\,\hat{s}_1 \\
&= \sqrt{\frac{\rho}{4M_t}}\mathbf{g}_1\Delta s + \sqrt{\frac{\rho}{4M_t}}\mathbf{g}_2 s_2 + \mathbf{n}_e \quad (25)
\end{aligned}$$

where $\Delta s = (s_1 - \hat{s}_1)$. The matched-filter $\mathbf{g}_2$ is used in detecting the symbol s_2 at the second stage. The channel instantaneous SINR is given by

$$\begin{aligned}
\gamma^E_{L2} &= \frac{\mathbb{E}|\mathbf{g}_2^H\,(\sqrt{\frac{\rho}{4M_t}}\mathbf{g}_2 s_2)|^2}{\mathbb{E}|\mathbf{g}_2^H(\sqrt{\frac{\rho}{4M_t}}\mathbf{g}_1\Delta s + \mathbf{n}_e)|^2} \\
&= \frac{\frac{\rho}{4M_t}|\mathbf{g}_2^H\mathbf{g}_2|^2}{\frac{\rho}{4M_t}|\mathbf{g}_2^H\mathbf{g}_1|^2\mathbb{E}|\Delta s|^2 + |\mathbf{g}_2^H\mathbf{g}_2|} \\
&\approx \frac{\frac{\rho}{4M_t}|\mathbf{g}_2^H\mathbf{g}_2|^2}{\frac{\rho}{4M_t}|\mathbf{g}_2^H\mathbf{g}_1|^2 d^2_{min} + |\mathbf{g}_2^H\mathbf{g}_2|} \quad (26) \\
&\approx \frac{(1-w\cos\theta)^2}{(w\sin\theta\,d_{min})^2} \triangleq \tilde{\gamma}^E_{L2} \quad (27)
\end{aligned}$$

where we obtain the approximation in (26) by replacing the square of the absolute value of the error with the square of the minimum distance d_{min} of the signal constellation. The approximation is made under the notion that symbol error occurs with highest probability to the nearest symbol in the constellation. We used high SNR approximation ($\rho \to \infty$) in (26) to reach the simple intuitive result of (27).

We simplify the channel instantaneous symbol error probability to

$$\mathcal{P}^{CSI}_{e|L1} = \left[\frac{4\mu}{\pi}\int_0^{\frac{\pi}{2}} - \frac{4\mu^2}{\pi}\int_0^{\frac{\pi}{4}}\right] e^{-\alpha_3(\phi)}d\phi \quad (28)$$

where $\alpha_3(\phi) \triangleq \frac{\delta\tilde{\gamma}^E_{L2}}{2\sin^2\phi}$. We next try to find the average symbol error probability at the second stage under the assumption that the detected symbol at the first stage with the MMSE filter is in error ($\hat{s}_1 \neq s_1$) over all channel realizations

$$\begin{aligned}
\mathcal{P}_{e|L1} &= \int_0^1\int_0^\infty \mathcal{P}^{CSI}_{e|L1} f_{\mathbf{a},\mathbf{w}}(a,w)\,da\,dw \\
&= \left[\frac{4\mu}{\pi}\int_0^{\frac{\pi}{2}}\int_0^1\int_0^\infty - \frac{4\mu^2}{\pi}\int_0^{\frac{\pi}{4}}\int_0^1\int_0^\infty\right] e^{-\frac{\delta\tilde{\gamma}^E_{L2}}{2\sin^2\phi}} f_{\mathbf{a},\mathbf{w}}(a,w)da\,dw\,d\phi \\
&= \left[\frac{4\mu}{\pi}\int_0^{\frac{\pi}{2}}\int_0^1\int_0^\infty - \frac{4\mu^2}{\pi}\int_0^{\frac{\pi}{4}}\int_0^1\int_0^\infty\right] I_3(a,w,\phi)\,da\,dw\,d\phi \\
&= \left[\frac{\mu\Gamma(4)}{\pi}\int_0^{\frac{\pi}{2}}\int_0^1 - \frac{\mu^2\Gamma(4)}{\pi}\int_0^{\frac{\pi}{4}}\int_0^1\right] \frac{(1-w^2)}{\Big[G_3(w,\phi)\Big]} dw\,d\phi \quad (29)
\end{aligned}$$

where $I_3(a,w,\phi) \triangleq e^{-\left[\frac{\delta(1-w\cos\theta)^2}{d^2_{min}\,w^2\,2\sin^2\phi\,\sin^2\theta}\right]}\left\{\frac{e^{-a}a^3(1-w^2)}{4}\right\}$, $G_3(w,\phi) \triangleq e^{\left[\frac{\delta(1-w\cos\theta)^2}{d^2_{min}\,w^2\,2\sin^2\phi\,\sin^2\theta}\right]}$. Using (17), (24), and (29), we can calculate directly $\mathcal{P}_{L2}$ by (18).

Having calculated $\mathcal{P}_{L1}$ by (17) and $\mathcal{P}_{L2}$ by (18), we can now obtain by (11) the approximate average block-error-rate for two symbols in the codeword that we denote $\mathcal{P}^{Approx}_{(s_1,s_2)}$. Due to the symmetry of the codeword transmission, the other pair of symbols represented by (s_3, s_4) has the same approximate block-error-rate as the pair (s_1, s_2). Hence, the approximate average block-error-rate for all 4 symbols in the codeword is given by

$$\mathcal{P}^{Approx}_{(s_1,\cdots,s_4)} = 2\mathcal{P}^{Approx}_{(s_1,s_2)} - \Big(\mathcal{P}^{Approx}_{(s_1,s_2)}\Big)^2. \quad (30)$$

Similarly, we can obtain an upper-bound in block-error-rate for the two symbols in the codeword by (17), (19), (24) and (11),

denoted by $\mathcal{P}^{\text{UB}}_{(s_1,s_2)}$ (Appendix C). An upper-bound average block-error-rate for the 4 symbols in the codeword is then

$$\mathcal{P}^{\text{UB}}_{(s_1,\cdots,s_4)} = 2\mathcal{P}^{\text{UB}}_{(s_1,s_2)} - (\mathcal{P}^{\text{UB}}_{(s_1,s_2)})^2. \tag{31}$$

Finally, we use the calculated approximate block-error-rate to optimize the code rotation angle θ in $\mathbf{P}_\theta$ in (1) for the given signal constellation $\mathcal{A}$,

$$\theta^* = \underset{\theta\in[0,\pi/2]}{\text{argmin}}\ \mathcal{P}^{Approx}_{(s_1,\cdots,s_4)}. \tag{32}$$

Certainly and unfortunately, closed form solution for the optimal rotation angle is not feasible. Yet, the easy to compute expression (30) makes it feasible to numerically obtain the optimal rotation angle.

V. Complexity and Performance Studies and Comparisons

In this section, we carry out computational complexity and error-rate performance comparisons of the proposed Hadamard precoded 4×4 QO-STBC with decoding as described in Section III (joint two-real-symbol ML or MMSE-MF) against the ML-decoded most powerful known to date 4×4 QO-STBC in [9] and [12].

In Table I, we present detailed complexity analysis and calculate the number of real multiplications and additions, denoted by $\mathbb{R}_M$ and $\mathbb{R}_A$ respectively, needed by the ML decoded codewords in [9], [12], [17] and our developed proposed QO-STBC with MMSE-MF decoding[2]. In all cases, we consider one receive antenna ($M_r = 1$). Implementation of linear detection has computational cost that is independent of constellation size. Of course, as the size of the signal constellation increases the cost of implementing the final symbol decision operator increases proportionally, as reflected on Table I. As expected, we observe that the computational complexity of the MMSE-MF decoder increases minimally with the constellation size, unlike [9], [12], and [17].[3] We can conclude that the proposed codeword/decoder combination reduces complexity drastically. What needs to be seen next is error-rate comparisons.

For error-rate studies we consider the 4 and 64-QAM signal constellation examples. For the proposed MMSE-MF decoder of the codeword in (1), (2), the block-error-rate minimizing rotation angle by (32) for 4 and 64-QAM is shown in Fig. 1 as a function of the SNR. The figure demonstrates the intriguing behavior of the rotation parameter under high-order (64 herein) symbol alphabets. For illustration purposes, in Fig. 2 we show the block-error-rate upper bound by (31), the approximate block-error-rate by (30), and the simulated block-error-rate of the proposed MMSE-MF decoded codeword with 4-QAM and 64-QAM alphabet and rotation angle fixed at 54° and 51.1°, respectively. These rotation angle values are the high-SNR converging points in Fig. 1 to enable open-loop system operation. We recall that the approximate block-error-rate expression encompasses two approximation steps, the high SNR assumption in (12) and d_{min}-type-only codeword errors in (26). In high alphabet sizes (e.g., 64-QAM compared to 4-QAM), non-d_{min}-type errors occur more frequently than low alphabet sizes in low/moderate SNR conditions. The relatively higher approximation error in the block-error-rate of 64-QAM in low SNR in Fig. 2 and higher rotation-angle dynamic range in low SNR in Fig. 1 may be attributed to the approximations in (12), (26).

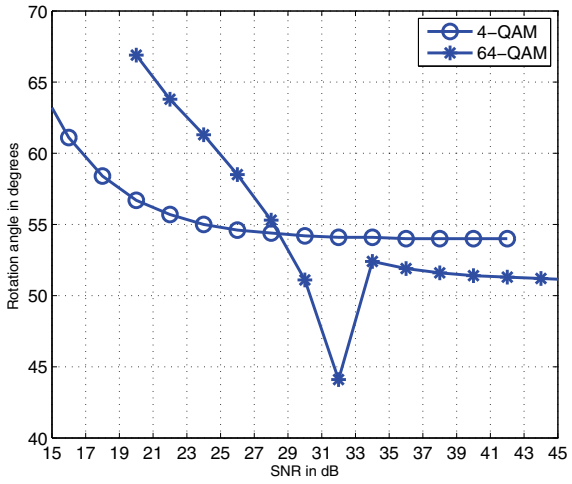

Fig. 1. Optimal rotation angle of proposed MMSE-MF decoded codeword versus SNR for the 4 and 64-QAM constellations.

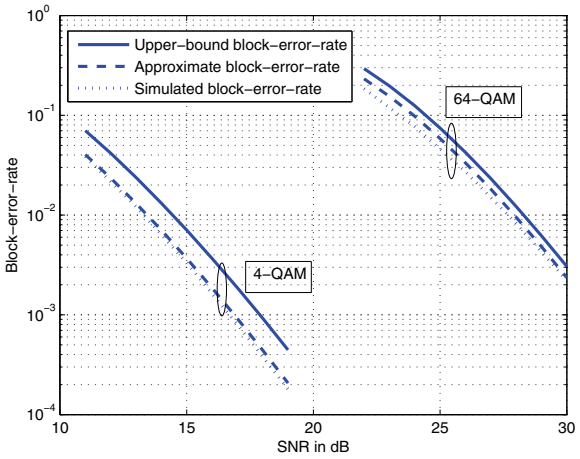

Fig. 2. Upper-bound, approximate, and simulated block-error-rate of proposed MMSE-MF decoded codeword versus SNR for the 4-QAM and 64-QAM constellation.

In Fig. 3, we fix the constellation size to 4-QAM and plot versus SNR the bit-error-rate of the codeword in (1), (2) under ML and MMSE-MF decoding, together with the bit error rates of the ML decoded codewords of [9], [12]. In Fig. 4, we repeat the study for 64-QAM.

In Fig. 5, we compare the bit-error-rate performance of the proposed codeword in (1), (2) and the codeword from [18] for $M_t = 4$ transmit antennas to be transmitted over $T = 6$ time slots that also employs linear decoding. For a fair comparison, the received SNR is set to be the same and the spectral efficiency is set to 2 bits per channel use for both

[2]We recall that the computational complexity of the proposed QO-STBC under ML decoding is the same as in [12].

[3]We have assumed that the SNR per receive antenna ρ is known at the receiver as is the case for [9], [12], and [17].

TABLE I
COMPARISONS OF REAL MULTIPLICATIONS AND ADDITIONS

QAM(L_R, L_I)	Code in (1),(2) MMSE-MF $\mathbb{R}_M, \mathbb{R}_A$	Code in [9] ML $\mathbb{R}_M, \mathbb{R}_A$	Code in [12] ML $\mathbb{R}_M, \mathbb{R}_A$	Code in [17] ML $\mathbb{R}_M, \mathbb{R}_A$
4 (2, 2)	283, 221	439, 451	512, 432	439, 451
16 (4, 4)	332, 225	3319, 4675	2048, 1728	592, 656
64 (8, 8)	348, 225	43639, 67651	8192, 6912	1744, 2192
256 (16, 16)	364, 225	665715, 1056835	32768, 27648	6352, 8336

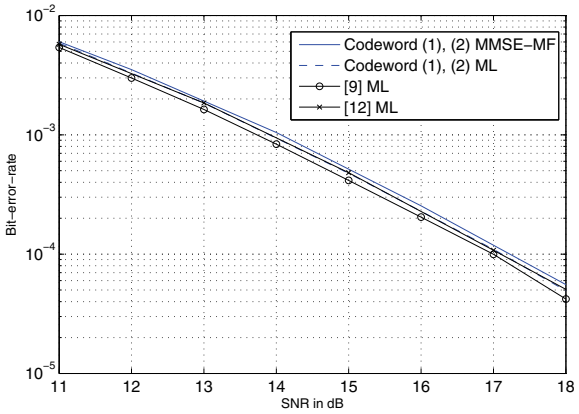

Fig. 3. Bit-error-rate versus SNR comparisons for 4-QAM constellation.

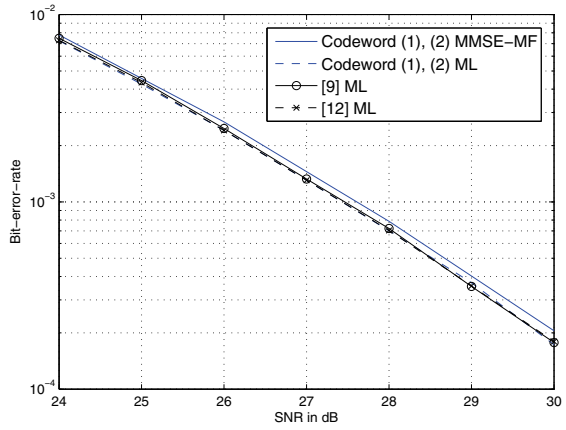

Fig. 4. Bit-error-rate versus SNR comparisons for 64-QAM constellation.

codewords.

In view of Figs. 3-5 and the complexity findings in Table I, the proposed precoded codeword and MMSE-MF decoder combination places itself as a strongest candidate for the preferred 4×4 space-time coding scheme.

VI. CONCLUSIONS

In 2×2 space-time block coding, the Alamouti code is the obvious choice with rate one, state-of-the-art error-rate performance, and minimal complexity. In this work, we set out to identify a 4×4 coding scheme that maintains rate one, matches closely the best known to date 4×4 error-rate performance, and has lowest computational complexity with minimal-only increase with the symbol alphabet size.

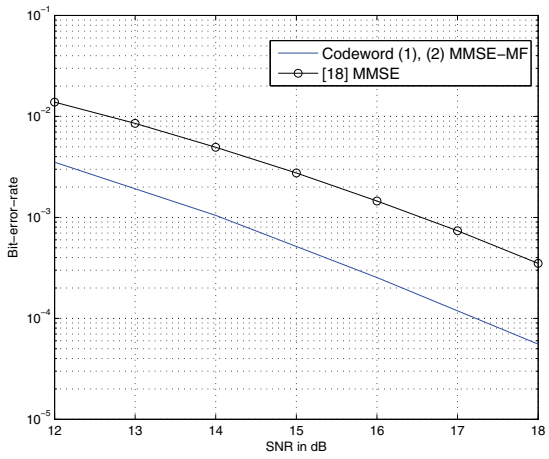

Fig. 5. Bit-error-rate versus SNR comparison of proposed rate-1 codeword with MMSE-MF decoding and 4-QAM constellation and rate-$2/3$ codeword of [18] with MMSE decoding and 8-QAM constellation (common spectral efficiency set to two bits per channel use).

The answer was given by Hadamard precoding that enables effective two-stage MMSE and MF linear filter decoding and MMSE-MF decoder block-error-rate rotation angle optimization. The proposed Hadamard precoded STBC with MMSE-MF decoding provides an excellent performance-versus-complexity operation point, which makes it a strong candidate as the 4×4 space-time block code of choice for field implementation. The described methodology may be extendable to higher code sizes using proportionally larger Hadamard[4] and rotation matrices as precoders.

APPENDIX A: EQUIVALENCE OF MMSE-MF, MMSE-MMSE, AND MMSE-ML DETECTORS

We denote the columns of the equivalent channel corresponding to the symbol pair (z_1, z_3) as $\mathbf{HV}_{[1,3]}\mathbf{J} \triangleq \left[\mathbf{g}_1\, \mathbf{g}_2\right]$. Assume that MMSE detectors are applied to both stages of the detection procedure. The MMSE filter at the second stage can be written as

$$\begin{aligned} \mathbf{w} &= \sqrt{\frac{\rho}{4M_t}}\left(\mathbf{I}_4 + \frac{\rho}{4M_t}\mathbf{g}_2\mathbf{g}_2^H\right)^{-1}\mathbf{g}_2 \\ &= \sqrt{\frac{\rho}{4M_t}}\mathbf{g}_2 - \sqrt{\frac{\rho}{4M_t}}\left(\frac{\mathbf{g}_2\mathbf{g}_2^H}{\frac{4M_t}{\rho} + \mathbf{g}_2^H\mathbf{g}_2}\right)\mathbf{g}_2 \\ &= \zeta\mathbf{g}_2 \end{aligned} \tag{33}$$

[4]A necessary condition for the existence of a Hadamard matrix is that its size is a multiple of four, [25].

where $\zeta = \frac{\sqrt{\frac{\rho}{4M_t}}}{1+\frac{\rho}{4M_t}\mathbf{g}_2^H\mathbf{g}_2}$.
Assume now correct detection at the first stage, i.e. $\hat{s}_1 = s_1$. When symbol detection at the first stage is correct, the signal processed at the second stage is given by (21). The SNR in this case is

$$\begin{aligned}\gamma^C_{MMSE} &= \frac{\mathbb{E}|\zeta\mathbf{g}_2^H(\sqrt{\frac{\rho}{4M_t}}\mathbf{g}_2 s_2)|^2}{\mathbb{E}|\zeta\mathbf{g}_2^H\mathbf{n}_e|^2} \\ &= \frac{\rho}{M_t}(a)(1-w\cos\theta) = \gamma^C_{L2}. \end{aligned} \quad (34)$$

Assume now incorrect detection at the first stage, i.e. $\hat{s}_1 \neq s_1$. When symbol detection at the first stage is incorrect, the signal processed at the second stage is given by (25). The SINR in this case is

$$\begin{aligned}\gamma^E_{MMSE} &= \frac{\mathbb{E}|\zeta\mathbf{g}_2^H(\sqrt{\frac{\rho}{4M_t}}\mathbf{g}_2 s_2)|^2}{\mathbb{E}|\zeta\mathbf{g}_2^H(\sqrt{\frac{\rho}{4M_t}}\mathbf{g}_1\Delta s+\mathbf{n}_e)|^2} \\ &= \frac{\frac{\rho}{4M_t}|\zeta\mathbf{g}_2^H\mathbf{g}_2|^2}{\frac{\rho}{4M_t}|\zeta\mathbf{g}_2^H\mathbf{g}_1|^2|\Delta s|^2+\zeta^2|\mathbf{g}_2^H\mathbf{g}_2|} \\ &= \gamma^E_{L2}. \end{aligned} \quad (35)$$

As both the MMSE-MF and MMSE-MMSE detectors have the same SNR/SINR at both stages, their error-rate performance is the same.

Consider now the case where ML detection is being used at stage two. For the additive Gaussian noise channel, ML detection performance is pre-detection SNR/SINR dependent. Under the assumption of correct detection at first stage ($\hat{s}_1 = s_1$), the pre-detection SNR ie equal to γ^C_{L2}. Under the assumption of incorrect detection at the first stage ($\hat{s}_1 \neq s_1$), it can be found that the pre-detection SINR is γ^E_{L2}.

We conclude that MMSE-MF, MMSE-MMSE, and MMSE-ML detector configurations are equivalent performance-wise. MMSE-MF has the lowest implementation complexity and is the obvious choice for practical use.

Appendix B: Proof of (16)

We derive the joint distribution of the channel parameters a and w. We define the variables

$$\begin{aligned} u^+ = u_R^+ + ju_I^+ &\triangleq (1/\sqrt{2})\cdot(h_1+h_3) &\sim\ & C\mathcal{N}(0,1), \\ u^- = u_R^- + ju_I^- &\triangleq (1/\sqrt{2})\cdot(h_1-h_3) &\sim\ & C\mathcal{N}(0,1), \\ v^+ = v_R^+ + jv_I^+ &\triangleq (1/\sqrt{2})\cdot(h_2+h_4) &\sim\ & C\mathcal{N}(0,1), \\ v^- = v_R^- + jv_I^- &\triangleq (1/\sqrt{2})\cdot(h_2-h_4) &\sim\ & C\mathcal{N}(0,1) \end{aligned}$$

where $C\mathcal{N}(0,1)$ is the complex Gaussian distribution with zero mean and unit variance and $u_R^{(\pm)}$, $u_I^{(\pm)}$, $v_R^{(\pm)}$, and $v_I^{(\pm)}$ are the real and imaginary parts of the corresponding complex random variables with each part being an independent and identically distributed real Gaussian random variable with mean zero and variance 0.5. Next, we define two new random variables used to obtain a and w, $Z_1 \triangleq |u^+|^2 + |v^+|^2 = u_R^{+2}+v_R^{+2}+u_I^{+2}+v_I^{+2}$ and $Z_2 \triangleq |u^-|^2+|v^-|^2 = u_R^{-2}+v_R^{-2}+u_I^{-2}+v_I^{-2}$. Z_1, Z_2 are independent and identically distributed with generalized Chi-square distribution. The joint distribution of Z_1 and Z_2 is

$$f_{Z_1,Z_2}(z_1,z_2) = z_1z_2e^{-(z_1+z_2)},\ z_1\in(0,\infty), z_2\in(0,\infty). \quad (36)$$

We now aim to find the joint distribution of a, w from the joint probability distribution of Z_1, Z_2 using a transformation. We observe that $a = Z_1+Z_2$, $w = \frac{|Z_1-Z_2|}{Z_1+Z_2}$. The joint probability density function of a, w is

$$f_{\mathbf{a},\mathbf{w}}(a,w) = \frac{f_{Z_1,Z_2}(z_1^{(1)},z_2^{(1)})}{|J(z_1^{(1)},z_2^{(1)})|} + \frac{f_{Z_1,Z_2}(z_1^{(2)},z_2^{(2)})}{|J(z_1^{(2)},z_2^{(2)})|} \quad (37)$$

where $z_1^{(1)} = (\frac{1+w}{2})a$, $z_2^{(1)} = (\frac{1-w}{2})a$, $z_1^{(2)} = (\frac{1-w}{2})a$, $z_2^{(2)} = (\frac{1+w}{2})a$ are the real roots of the transformations and $J(\cdot,\cdot)$ is the Jacobian matrix. Simplifying (37), we obtain the elegant pdf expression

$$f_{\mathbf{a},\mathbf{w}}(a,w) = \frac{1}{4}(1-w^2)a^3e^{-a},\ a\in(0,\infty), w\in(0,1). \quad (38)$$

Appendix C: Proof of (31)

We denote the symbol error-rate at the first stage at SINR γ_{L1} and $\tilde{\gamma}_{L1}$ by $\mathcal{P}_{L1}(\gamma_{L1})$ and $\mathcal{P}_{L1}(\tilde{\gamma}_{L1})$, respectively. It can be shown utilizing (12) that $\tilde{\gamma}_{L1} \leq \gamma_{L1}$, which implies $\mathcal{P}_{L1}(\gamma_{L1}) \leq \mathcal{P}_{L1}(\tilde{\gamma}_{L1})$. From (11), we have

$$\begin{aligned}\mathcal{P}_{(s_1,s_2)} &= \mathcal{P}_{L1}+\mathcal{P}_{L2}(1-\mathcal{P}_{L1}) \\ &\leq 2\mathcal{P}_{L1}+\mathcal{P}_{e|\overline{L1}}(1-\mathcal{P}_{L1})^2-\mathcal{P}_{L1}^2 \end{aligned} \quad (39)$$

The right hand side of (39) is an increasing function of $\mathcal{P}_{L1}$. Combining (39) and $\mathcal{P}_{L1}(\gamma_{L1}) \leq \mathcal{P}_{L1}(\tilde{\gamma}_{L1})$, we obtan $\mathcal{P}_{s_1,s_2} \leq \mathcal{P}^{\text{UB}}_{s_1,s_2}$.

Acknowledgement

The authors would like to thank the Associate Editor Michail Matthaiou and the four anonymous reviewers for their comments and suggestions that helped improve this manuscript significantly, both in presentation and content.

References

[1] V. Tarokh, H. Jafarkhani, and A. R. Calderbank, "Space-time block codes from orthogonal designs," *IEEE Trans. Inf. Theory*, vol. 45, pp. 1456–1467, May 1999.
[2] S. Alamouti, "A simple transmit diversity technique for wireless communications," *IEEE J. Sel. Areas Commun.*, vol. 16, pp. 1451–1458, Aug. 1998.
[3] W. Su and X.-G. Xia, "On space-time block codes from complex orthogonal designs," *Wireless Pers. Commun.*, vol. 25, no. 1, pp.1–26, Apr. 2003.
[4] H. Jafarkhani, "A quasi-orthogonal space-time block code," *IEEE Trans. Commun.*, vol. 49, pp. 1–4, Jan. 2001.
[5] O. Tirkkonen, A. Boariu, and A. Hottinen, "Minimal non-orthogonality rate 1 space-time block code for 3+ Tx antennas," in *Proc. 2000 IEEE Int. Symp. Spread-Spectrum Techniques Apps.*, pp. 429–432.
[6] E. Biglieri, Y. Hong, and E. Viterbo, "On fast-decodable space-time block codes," *IEEE Trans. Inf. Theory*, vol. 55, pp. 524–530, Feb. 2009.
[7] K. Pavan Srinath and B. Sundar Rajan, "Low ML-decoding complexity, large coding gain, full-rate, full-diversity STBCs for 2×2 and 4×2 MIMO systems," *IEEE J. Sel. Topics Signal Process.*, vol. 3, pp. 916–927, Dec. 2009.
[8] T. P. Ren, Y. L. Guan, C. Yuen, E. Gunawan, and E. Y. Zhang, "Group decodable space-time block codes with code rate >1," *IEEE Trans. Commun.*, vol. 59, pp. 987–997, Apr. 2011.
[9] W. Su and X. G. Xia, "Signal constellations for quasi-orthogonal space-time block codes with full diversity," *IEEE Trans. Inf. Theory*, vol. 50, pp. 2331–2347, Oct. 2004.

[10] N. Sharma and C. B. Papadias, "Improved quasi-orthogonal codes through constellation rotation," *IEEE Trans. Commun.*, vol. 51, pp. 332–335, Mar. 2003.
[11] Z. A. Khan, B. S. Rajan, and M. H. Lee, "Rectangular co-ordinate interleaved orthogonal designs," in *Proc. 2003 IEEE GLOBECOM*, vol. 4, pp. 2004–2009.
[12] C. Yuen, Y. L. Guan, and T. T. Tjhung, "Quasi-orthogonal STBC with minimum decoding complexity," *IEEE Trans. Wireless Commun.*, vol. 4, pp. 2089–2094, Sep. 2005.
[13] H. Wang, D. Wang, and X.-G. Xia, "On optimal quasi-orthogonal space-time block codes with minimum decoding complexity," *IEEE Trans. Inf. Theory*, vol. 55, pp. 1104–1130, Mar. 2009.
[14] W. Liu, M. Sellathurai, P. Xiao, and J. Wei, "A new restricted full-rank single-symbol decodable design for four transmit antennas," *IEEE Signal Process. Lett.*, vol. 15, pp. 765–768, Nov. 2008.
[15] C. Yuen, Y. L. Guan, and T. T. Tjhung, "Optimizing quasi-orthogonal STBC through group-constrained linear transformation," *IET Commun.*, vol. 1, pp. 373–381, June 2007.
[16] T. P. Chen, Y. L. Guan, C. Yuen, and E. Y. Zhang, "Block-orthogonal space-time code structure and its impact on QRDM decoding complexity reduction," *IEEE J. Sel. Topics Signal Process.*, pp. 1438–1450, Dec. 2011.
[17] L. Azzam and E. Ayanoglu, "Maximum likelihood detection of quasi-orthogonal space-time block codes: analysis and simplification," in *Proc. 2008 IEEE Int. Conf. Commun.*, pp. 3948–3954.
[18] Y. Shang and X.-G. Xia, "Space-time block codes achieving full diversity with linear receivers," *IEEE Trans. Inf. Theory*, vol. 54, pp. 4528–4547, Oct. 2008.
[19] G. S. Rajan and B. S. Rajan, "MMSE optimal algebraic space-time codes," *IEEE Trans. Wireless Commun.*, vol.7, pp. 2468–2472, July 2008.
[20] X. Guo and X.-G. Xia, "On full diversity space-time block codes with partial interference cancelation group decoding," *IEEE Trans. Inf. Theory*, vol. 55, pp. 4366–4385, Oct. 2009.
[21] A. Sezgin and T. J. Oechtering, "Complete characterization of the equivalent MIMO channel for quasi-orthogonal space-time codes," *IEEE Trans. Inf. Theory*, vol. 54, pp. 3315–3326, July 2008.
[22] W. Su, S. N. Batalama, and D. A. Pados, "On orthogonal space-time block codes and transceiver signal linearization," *IEEE Commun. Lett.*, vol. 10, pp. 91–93, Feb. 2006.
[23] M. K. Simon and M.-S. Alouini, *Digital Communication over Fading Channels: A Unified Approach to Performance Analysis.* Wiley, 2000.
[24] I. S. Gradshteyn and I. M. Ryzhik, *Table of Integrals, Series, and Products*. Academic Press, 1980.
[25] H. Ganapathy, D. A. Pados, and G. N. Karystinos, "New bounds and optimal binary signature sets—part II: aperiodic total squared correlation," *IEEE Trans. Commun.*, vol. 59, pp. 1411–1420, May 2011.

Sandipan Kundu received his B.S. and M.S. degrees in electrical engineering from the State University of New York at Buffalo in 2006 and 2008, respectively. He is currently a Ph.D. candidate and member of the Communications, Signal Processing, and Networking Research Group, Dept. of Electrical Engineering, State University of New York at Buffalo.

His research interest includes space-time coding, low-complexity multi-antenna, multi-user detection, physical layer secrecy, cognitive radio, and optimization of wireless feedback protocols. He was a recipient of the University at Buffalo's Graduate Presidential Fellowship and a Motorola Senior Scholar Award.

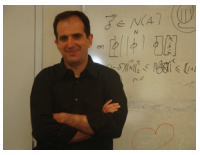

Dimitris A. Pados (M'95) was born in Athens, Greece, on October 22, 1966. He received the Diploma degree in computer science and engineering (five-year program) from the University of Patras, Greece, in 1989, and the Ph.D. degree in electrical engineering from the University of Virginia, Charlottesville, VA, in 1994.

From 1994 to 1997, he held an Assistant Professor position in the Department of Electrical and Computer Engineering and the Center for Telecommunications Studies, University of Louisiana, Lafayette. Since August 1997, he has been with the Department of Electrical Engineering, State University of New York at Buffalo, where he is presently a Professor. He served the Department as Associate Chair from 2009–2010. Dr. Pados was elected three times as a University Faculty Senator (terms 2004–2006, 2008–2010, and 2010–2012) and served on the Faculty Senate Executive Committee from 2009–2010.

His research interests are in the general areas of communication theory and adaptive signal processing with applications to interference channels and signal waveform design, secure wireless communications, cognitive radios, and networks.

Dr. Pados is a member of the IEEE Signal Processing, Communications, Information Theory, and Computational Intelligence Societies. He served as an Associate Editor for IEEE SIGNAL PROCESSING LETTERS from 2001 to 2004 and the IEEE TRANSACTIONS ON NEURAL NETWORKS from 2001 to 2005. He received a 2001 IEEE International Conference on Telecommunications best paper award, the 2003 IEEE TRANSACTIONS ON NEURAL NETWORKS Outstanding Paper Award, and the 2010 IEEE International Communications Conference Best Paper Award in Signal Processing for Communications for articles that he co-authored with students and colleagues. Professor Pados is a recipient of the 2009 SUNY-system-wide Chancellor's Award for Excellence in Teaching and the 2011 University at Buffalo Exceptional Scholar - Sustained Achievement Award.

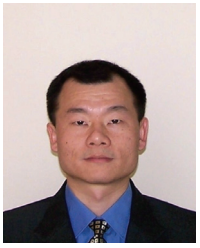

Weifeng Su (M'03) received the Ph.D. degree in electrical engineering from the University of Delaware, Newark, DE, in 2002. He received his B.S. and Ph.D. degrees in mathematics from Nankai University, Tianjin, China, in 1994 and 1999, respectively. His research interests span a broad range of areas from signal processing to wireless communications and networking, including MIMO wireless communications, space-time coding and modulation, transceiver designs, and cooperative communications for wireless networks.

Dr. Su joined the Department of Electrical Engineering at the State University of New York (SUNY) at Buffalo in 2005, where he is currently an Associate Professor. From June 2002 to March 2005, he was a Postdoctoral Research Associate with the Department of Electrical and Computer Engineering and the Institute for Systems Research, University of Maryland, College Park, MD. Dr. Su is the recipient of the 2010 IEEE International Conference on Communications (ICC) Best Paper Award. He received the Invention of the Year Award from the University of Maryland in 2005. He received the Signal Processing and Communications Faculty Award from the University of Delaware in 2002. Dr. Su has been serving as Editor for the IEEE TRANSACTIONS ON WIRELESS COMMUNICATIONS since January 2012. He served as Associate Editor for the IEEE TRANSACTIONS ON VEHICULAR TECHNOLOGY from 2005 to 2009 and IEEE SIGNAL PROCESSING LETTERS from 2007 to 2012. He also co-organized two Special Issues for IEEE journals in the fields of cooperative communications and networking. Dr. Su co-authored the book *Cooperative Communications and Networking* published by Cambridge University Press in 2009.

Rohan Grover received his B.E. in electrical and electronics engineering from Bangalore University, India in 2001, and the M.S. and Ph.D. in electrical engineering in 2004 and 2007, respectively, from the University at Buffalo, State University of New York, NY.

From July 2007 to November 2008, he was a Senior Communications Systems Engineer at Radiospire Networks, a VC funded start-up in the Greater Boston area, where he was involved in developing algorithms for RF impairment mitigation for a gigabit OFDM system over ultra wideband channels. He is currently working with Mirics Software, which develops software defined radio solutions for television and radio broadcast signals for x86 and ARM chipsets. Over the last 4 years, he has worked on demodulation and decoding algorithms for standards ATSC, 256 Cable-QAM, DVB-T, ISDB-T, and DAB.